



State-of-the-Art Gamma-Ray Spectrometers for In-Beam Measurements

5

Francesco Recchia and Caterina Michelagnoli

Abstract

High-resolution γ -ray spectroscopy is one of the most powerful and sensitive tools to investigate nuclear structure. Significant progress in this field has been achieved through the use of arrays of Compton-suppressed high-purity germanium detectors; however, it is apparent that such devices are not suited to the expected experimental conditions at the planned and under construction radioactive ion beam facilities. Devices with higher efficiency and sensitivity have been developed during the past two decades relying on the possibility to determine the position and the energy deposition of the individual interaction points of a photon within a germanium crystal and on the capability to reconstruct the photon scattering sequence through powerful data analysis algorithms. In these notes a brief introduction to the principles of γ -ray tracking arrays will be given. After a historical overview of the main spectrometers that contributed to the present understanding of the nuclear structure, the principles of advanced γ -ray tracking will be described. A basic technical description of arrays based on this technique will be reported together with some selected results.

F. Recchia (✉)
University and INFN Padova, Padova, Italy
e-mail: francesco.recchia@unipd.it

C. Michelagnoli
Institut Laue-Langevin, Grenoble, France
e-mail: cmichela@ill.eu

5.1 Introduction

Since germanium detectors became available in the 1960s, they constituted the most used and important tool for γ -ray spectroscopy. In particular, the modern High-Purity Germanium crystals (HPGe) provide an excellent (1–3 keV) energy resolution in the typical energy range for nuclear spectroscopic studies that ranges between approximately 10 keV and 10 MeV. The continuous development of high-resolution γ -ray detector systems has been of vital importance to nuclear structure physics. It has steadily expanded the limits of what can be observed, allowing for the discovery of new phenomena and leading to deeper insights into the nature of the nucleus. Indeed, large arrays of HPGe detectors became in the 1990s the state-of-the-art instruments for γ -ray spectroscopy, having not only a large photo-peak efficiency, but also allowing high selectivity of the reaction channels of interest, through the analysis of multiple γ coincidences. The key concept behind these arrays is to obtain the required selectivity (and efficiency) through the combination of several detectors, each of them with good response function (in other words, with energy resolution and ratio of peak over total, P/T ratio, both as good as possible). It should be strongly remarked that since, in in-beam γ -ray spectroscopy, the photons are emitted by recoiling nuclei, the FWHM of the peak is dominated in most cases by the Doppler broadening due to the finite size of the detector, rather than the intrinsic detector resolution. This means that each element of the array should cover a solid angle as small as possible to keep this broadening within “reasonable” limits. Concerning the P/T ratio, the background generated by partially absorbed photons can be the dominant part of the spectrum for the available size of the HPGe crystals. Such background can be efficiently reduced by surrounding the Ge detectors with the so-called Compton suppression shields, namely, veto detectors that detect photons escaping from the germanium crystal. A major breakthrough in the field of γ -spectroscopy was achieved in the 1990s with the construction of arrays of Compton-shielded large-volume HPGe detectors GASP [1, 2], EUROGAM [3], EUROBALL [4], and GAMMASPHERE [5]. In principle, an array of germanium detectors should have as large as possible photopeak efficiency, in order to limit the time needed to acquire the required statistics to a minimum. Large photopeak efficiency is best obtained by combining several detectors, each of them subtending a small solid angle. In this way, not only the Doppler broadening effects is kept under control but also the probability of multiple hits, i.e., two or more photons entering the same crystal at the same time are minimized. Multiple-hit phenomena can be significant when several photons are emitted simultaneously. The characteristics to be considered to assess the quality of an array of HPGe detectors for high-resolution and high-efficiency in-beam γ -ray spectroscopy can thus be summarized as follows:

- effective energy resolution;
- full-energy (photopeak) efficiency;
- peak-to-total ratio;

- granularity;
- amount of dead materials;
- time resolution;
- counting-rate capabilities.

With the “conventional” Compton suppression techniques, it was not feasible to reach simultaneously total photopeak efficiencies around 50% and P/T ratios around 50%. These two parameters are considered essential features to pursue the physics program at radioactive ion beam facilities [6]. An alternative approach, followed since the 1990s [7], involves the construction of a Ge ball around the target position, with the development of techniques (pulse shape analysis and γ -ray tracking) to “look inside” the germanium crystals and to follow the individual photon scattering.

In these notes the concept of *advanced γ -ray tracking* will be introduced, together with the main subjects connected to this technique. Before going into the details of this detection technique, the composite detector technology, such as clover and cluster, will be briefly discussed. This technology is indeed in use in many facilities and provides still nowadays many advantages.

5.1.1 Clovers and Add-Back Procedure

Following the above discussion, it is clear that in developing an array of HPGe detectors, a careful balance must be found between two contrasting needs. On one hand the detectors should be placed at large distances from the target position in order to subtend small solid angles with each element. As it will be explained in detail in Sect. 5.3, the effective energy resolution strongly depends on the uncertainty on the direction of the γ -ray as a consequence of the Doppler shift of the γ -rays emitted by nuclei recoiling after a nuclear reaction. Thus to obtain a reasonable resolution, it is important that each detector subtend a small angle. On the other hand, in order to maximize the detection efficiency with a given number of detectors, each of them should be placed as close as possible to the target position. The problem can be partially overcome by using composite detectors such as the clover [8] and cluster [9] detectors developed within the EUROBALL collaboration. In these detectors, more crystals (respectively, 4 and 7) share the same cryostat and the same Compton-suppression shield. Efficiency and peak-to-total can be recovered by summing up (adding back) the energy deposited in neighboring detectors.

Clover-based arrays are used in γ -ray spectroscopy in international facilities [10–12]. The working principle of Compton-suppressed clover detectors is schematized in Fig. 5.1. When γ -rays are detected in coincidence by different crystals in a clover, their energies are “added-back” in order to recover the full energy of the original γ ray. This is exemplified in Fig. 5.2 where the spectra corresponding to the energy measured by individual crystals is compared to the spectra corresponding to the energy resulted from the add-back of all the crystals in a clover detector. Because of the electrical coupling within the cryostat of the clover detector, the channels suffer a relevant cross talk that implies that the energy obtained by summing the

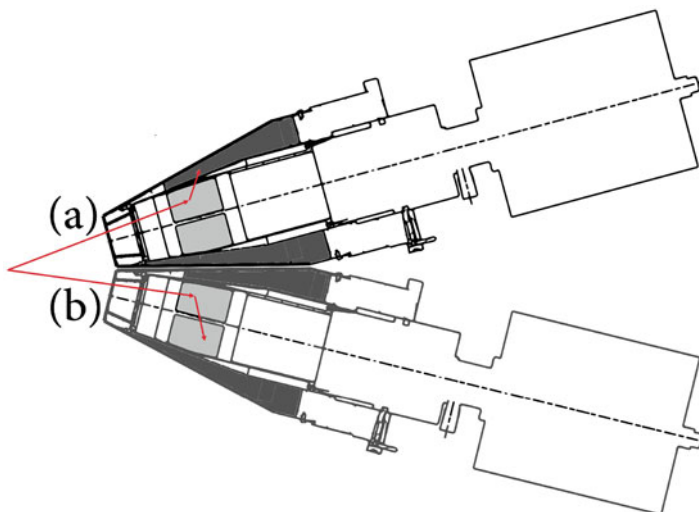


Fig. 5.1 Two clover detectors with the anti-Compton shield. The γ -ray labeled (a) scatters in one germanium crystal, and it is absorbed by the anti-Compton shield resulting in a rejected event. The γ -ray labeled (b) scatters in one germanium crystal, and it is absorbed by a neighboring germanium crystal resulting in a full-energy count in the add-back spectrum

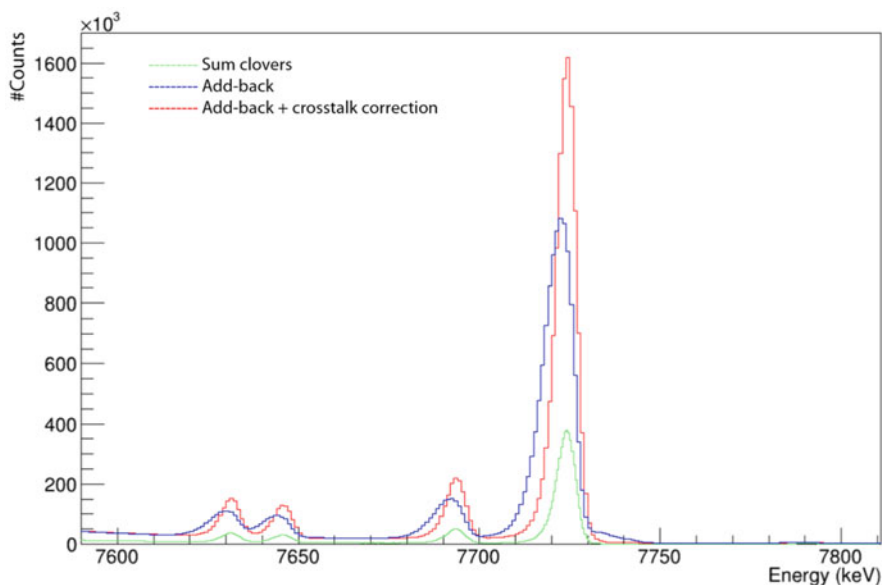


Fig. 5.2 Spectrum obtained with the $^{27}\text{Al}(n,\gamma)^{28}\text{Al}$ reaction with the clover array FIPPS at ILL. In green, spectrum obtained using each single crystal separately; in blue, spectrum obtained using the add-back procedure within each clover detector; in red, add-back spectrum obtained using the add-back procedure and applying a cross talk correction. Taken from [13]

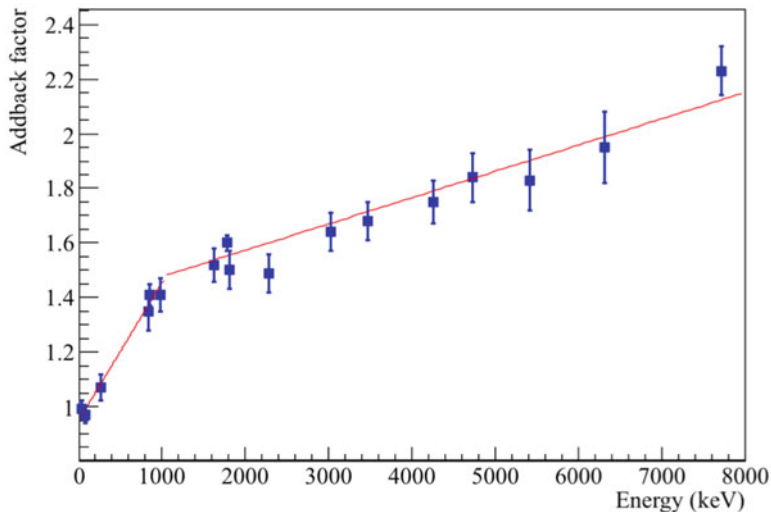


Fig. 5.3 Add-back factor as a function of the energy for the FIPPS clover array at the Institut Laue-Langevin (ILL). See text for more details. Taken from [14]

ones detected by two or more crystals has a deficit that needs to be corrected. The importance of the cross talk is highlighted by the comparison between the add-back spectrum with and without cross talk correction reported in Fig. 5.3.

In Fig. 5.3 the add-back factor as a function of the energy is reported for the FIPPS spectrometer at the Institut Laue-Langevin (ILL), as an example of the importance of add-back for the performance of a clover array. The add-back factor is determined from the ratio of the area of the peak after add-back and the one in the spectrum obtained as sum of all detectors (without add-back). The data in the picture are obtained from (n,γ) reactions on Al and Mn targets. The result of a linear fit is reported. The change of slope at ≈ 1 MeV is due to the occurrence of pair production. While the gain in full-energy peak efficiency is evident, especially at high energy, the capabilities of such devices are limited by the following factors:

- Uncertainty in the direction of the γ -ray due to the finite size of the detector: the direction of the γ used for Doppler correction and angular correlations/distributions is assumed to correspond to the one of the crystal with the largest energy deposit. There is no information about where the interaction took place within a crystal. The dimension of a detector and its distance to the target are thus defining how precisely the direction of the γ ray is known;
- In case the γ scatters from one crystal to a neighboring one, given that the sequence in the Compton scattering is only guessed, systematic errors are done in the extraction of observables that require such information (first, second interaction point);

- At high count rate, summing effects can occur (two distinct γ rays are accidentally added-back).
- Eventual nonlinearities in the energy calibrations or cross talk effects (not properly corrected) may affect the resolution in the energy spectrum after add-back. In Fig. 5.2 a comparison of the energy resolution under different conditions is shown. In particular, the effect of cross talk correction is evident.

5.2 Advanced γ -Ray Tracking

5.2.1 General Aspects: The Tracking Concept

The state-of-the-art γ -ray detector arrays aim at overcoming the main limitations of traditional arrays, namely, the “finite” detector size/position resolution and efficiency. γ -Ray tracking arrays, exploiting the position sensitivity obtainable from segmentation of the outer contact of the detector, can achieve a major step forward both in Doppler correction capabilities and in efficiency. The idea is thus to build 4π detector arrays composed entirely of HPGe, as shown in Fig. 5.4, that will be used not simply in a calorimetric mode but instead will allow to reconstruct the path of each γ -ray inside the detector volume. As it will be shown in the following, such a device is highly demanding and challenging in terms of performance and technology. Nowadays two projects exist, one in Europe named AGATA [15], one in the USA, named GRETA [16].

The idea at the basis of the *advanced γ -ray tracking* is to reconstruct the individual γ -ray energies and directions, based on the deposited energy and position

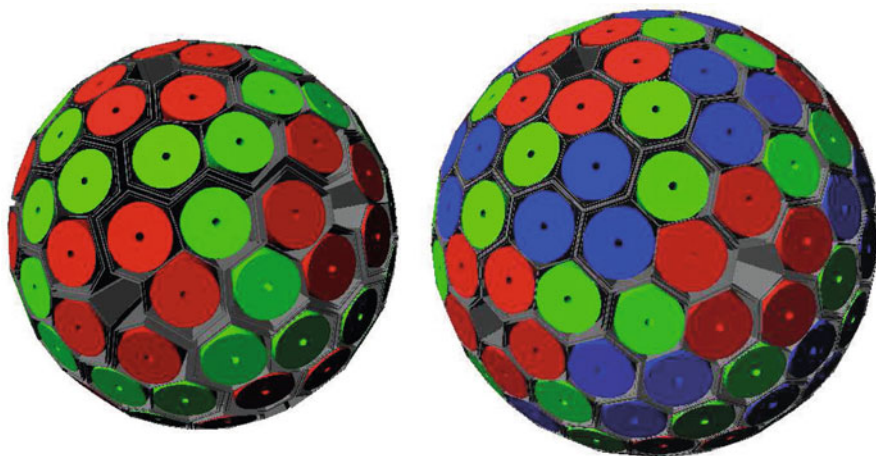
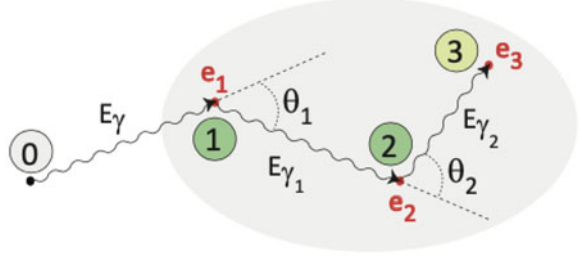


Fig. 5.4 Artistic view of the γ -ray tracking arrays GRETA (120 crystals, left) and the AGATA (180 crystals, right). The colors correspond to different germanium crystal shape tapered in irregular hexagon to guarantee an optimal solid angle coverage

Fig. 5.5 Schematic representation of a photon that undergoes two interactions



of all the interaction points of an event seen by the detector(s). For each event, the number of photons, their energies, the incident, and scattering directions should be measured, and the events corresponding to incomplete energy release should be discarded. In principle, this could be done by knowing the interaction positions with sufficient precision and the details of the interaction mechanisms. In the energy range between 100 keV and 10 MeV, γ rays interact with Ge mainly via Compton scattering [17]. In the limit of a free electron at rest, this process is analytically described by (5.1):

$$E_{\gamma i} = \frac{E_{\gamma i-1}}{\frac{E_{\gamma i-1}}{m_e c^2} (1 - \cos \theta_i)} \quad (5.1)$$

where $E_{\gamma i}$ is the energy of the γ -ray after the i -th scattering.

Above 1.022 MeV, the γ energy is sufficient for creating an e^+e^- pair, with the positron later annihilating and emitting two 511 keV photons in opposite directions. To clarify the basic concepts behind the technique of γ -ray tracking, let us consider a photon that undergoes two interactions before being absorbed, as shown in Fig. 5.5. Assuming the electrons in the material unbound and at rest, the energy is related to the scattering angle by (5.1). If the source position is known, one can evaluate the Compton formula for each permutation of the interaction points and build a χ^2 function (figure of merit) of the kind:

$$\chi^2 \approx \sum_{n=1}^{N-1} w^n \left(\frac{E_{\gamma'} - E_{\gamma'}^{Pos}}{E_{\gamma}} \right)_n^2 \quad (5.2)$$

Recalling that the initial photon energy E_{γ} is the sum of the individual deposited energies, and assuming a given sequence for the photon scattering, the photon energy after the i th scattering is easily computed as:

$$E_{\gamma'} = E_{\gamma} - \sum_{n=1}^i e_n \quad (5.3)$$

$E_{\gamma i}$ can also be computed starting from (5.1). In practice, a figure of merit should be evaluated for all the possible permutations of the interaction points. The event is accepted only if the merit of the best permutation is lower than an empirically defined limit. The discarded events are the “software equivalent” of a Compton suppression. The analysis of all partitions of the measured points for (real) cases of more than one γ per event is normally not feasible (10^{23} partitions for 30 points). The interactions of single photons must be thus grouped by means of clustering techniques [18]. The points generated by a single γ are expected to be localized in a small portion of the total detector volume, compatible with the finite absorption length for the photons and with the forward peaking of the Compton scattering. The interactions belonging to the same track can be clustered on the basis of the angular separation (seen from the source) and their mutual linear distance.

The tracking algorithms can be distinguished in two classes: forward- and back-tracking [19, and references therein]. Using the backtracking method, the interaction points within a given deposited energy interval are considered as last interactions of fully absorbed γ rays. The scattering is then tracked backwards, back to the known position of the source.

The forward tracking method, instead, starts from the identification of a set of clusters, each identified by its energy, sum of the energy depositions in the cluster. The three interaction mechanisms of γ rays in germanium are then tested, and “good clusters” are selected via a χ^2 test. The fundamental effects limiting the performance of the tracking algorithms can be summarized as follows:

- difference between the position of the photon interaction and the one of the energy deposition (electrons drift)
- electrons energy loss via bremsstrahlung
- Rayleigh scattering of low-energy γ rays toward the end of a track (change of direction without change of energy)
- (5.1) is just an approximation; electrons in media are not free nor at rest; the formula should be corrected in order to take the momentum of the electron into account.

All the abovementioned effects are “masked” by the error in the determination of the interaction points. Indeed important uncertainties are introduced by the determination of the interaction points, position resolution, energy threshold, and the presence of dead materials.

The concept of γ -ray tracking can be summarized as represented in Fig. 5.6.

In order to track the γ -ray scattering path, it is necessary to use the detectors in position-sensitive mode. This is described in the next section.

5.2.2 Pulse Shape Analysis

The shape of the signal in a true coaxial detector depends on the distance of the interaction to the central contact [17]. Given the cylindrical symmetry of the system,

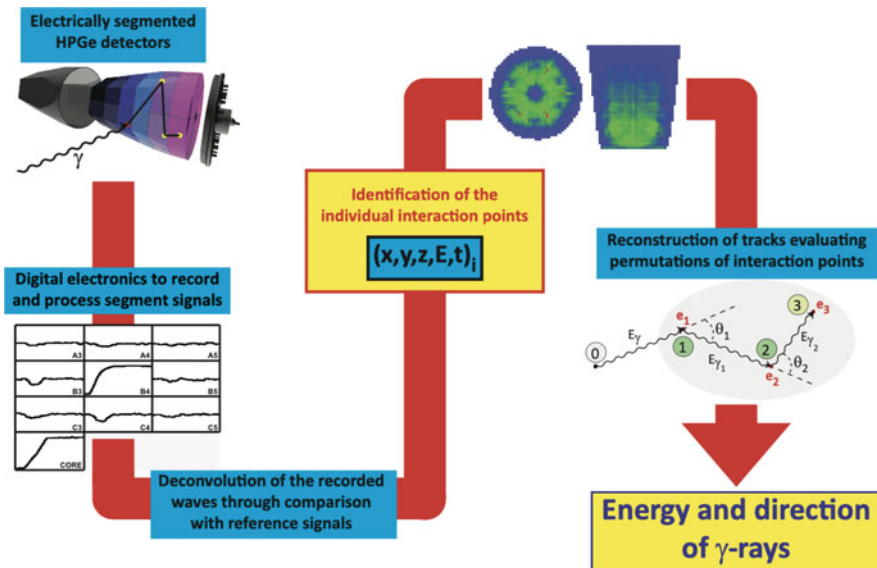


Fig. 5.6 Main steps for the tracking of γ -rays detected by HPGe segmented detectors. The picture summarizes all the different steps detailed in the text

no other information on the position can be extracted, unless this symmetry is broken, for example, by electrically segmenting one of the electrodes. When one of the electrodes is electrically segmented, the motion of the charges within one segment induces signals also in the neighboring electrodes (Fig. 5.7). Contrary to the segment where the interaction takes place (i.e., where there is a net charge release), the total collected charge in the neighboring electrodes is zero. For this reason, the signals induced in the neighboring electrodes are known as *transient signals*. The shapes and amplitudes of net and transient shapes depend also on the angular position of the interaction point, as exemplified in Fig. 5.7. The amplitude of the induced transient signals provides a convenient way to locate the interaction with sub-segment precision, but this is not enough to achieve the required position resolution. In order to reach a better precision, the full shapes of the observed signals should be compared to a set of reference signals, each of them corresponding to interactions taking place in well-defined locations in the crystal. In principle, the basis of reference signals for a given segmented detector should be constructed experimentally, measuring in a semi-automatic way the signals corresponding to specific locations within the crystal, with the possibility to move such locations in any point of the detector. This can be done using collimated γ -ray sources and coincidence detectors to construct what is known as *scanning tables* [20, 21]. However, obtaining scanned bases for all the detectors of an array is extremely time-consuming and in practice not feasible, and as a consequence techniques to

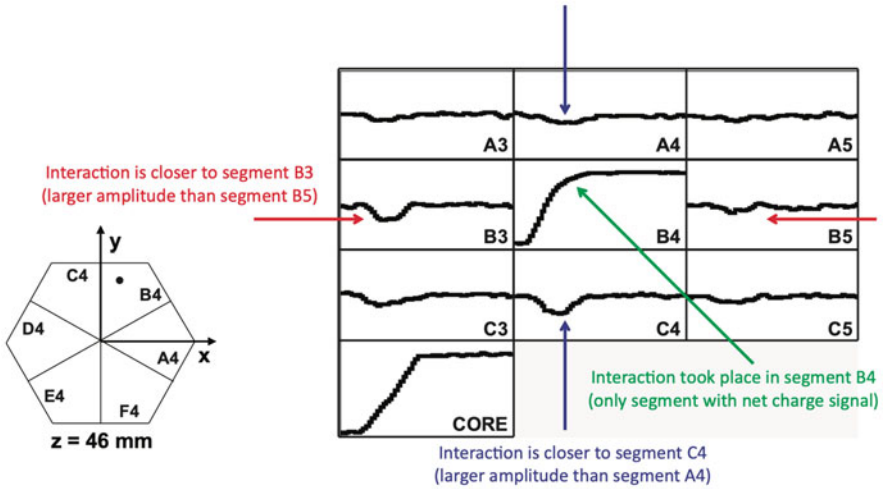


Fig. 5.7 Segment signal shapes following a γ -interaction in one segment at 46 mm depth in an AGATA segmented HPGe. The net charge signal identifies the segment where the interaction took place, while the amplitude of the transient signals suggests its position inside the segment

calculate these reference signals have been developed, with parameters adjusted by comparison with measured pulse shapes in “key-locations” in the crystal [22].

In principle, the knowledge of the electric field (or potential) in the full segmented detector would be required for such calculations. This is quite a complicated problem, that is why, in practice, the Shockley-Ramo theorem is used as a simplification [23, and references therein]. The *weighting field* is calculated for each sensing electrode by solving numerically the Laplace equation with the sensing electrode put at fixed potential while grounding all the others. The Ramo theorem guarantees a direct relation between the charge released in a given position inside the crystal and the weighting potential at that position. For an AGATA detector, which has a 6x6 outer segmentation, the calculation requires the solution of 1 Poisson and 37 Laplace (1 anode and 36 cathodes) equations. The calculated basis is usually considered on a space grid of 1 mm and a time step of 1 ns. Once the reference signal basis is available, the interaction points of the detected γ radiation into the germanium detector are obtained by comparison with the recorded waveforms (an example of detector signal is reported in Fig. 5.7), and this is called pulse shape analysis (PSA). The quality of this procedure strongly determines the performance of the tracking algorithm and depends mainly on two factors, additional to the quality of the signal basis:

- proper handling of the signals to correct for second-order effects due to electronic couplings among the channels
- performance of the algorithm used to make the comparison.

Assuming a “perfectly performing” PSA algorithm, still the experimental waveforms are not at all “ideal,” and signal distortions could result in a displacement of the reconstructed interaction point from the actual one. Apart from the electronic noise that has to be minimized by means of proper grounding of the electronics, some other effects can be observed and taken into account/corrected in the data preparation to the PSA.

In any electrically segmented detector, the cross talk phenomenon is present. It produces a shift in the reconstructed energies that is proportional to the segment fold of the event, namely, to the number of segments firing simultaneously. The origin and calculations for the correction of this effect are extensively described in [23, 24]. The cross talk affects the detector energy resolution since the gain varies depending on the pattern of firing segments. The amplitude of a signal from one segment has therefore to be corrected according to a linear combination of the signal amplitudes of the other segments. Experimentally, two kinds of cross talk have been observed: a cross talk which is proportional to the net-charge signal and one which is proportional to its time derivative. Measurements of both kinds of cross talk are reported in [23]. The PSA algorithm compares the measured signals with a reference basis of simulated single interaction signals. This algorithm has to effectively identify the interaction points in the crystal and efficiently process the experimental data in order to obtain the positions and energy depositions from the experimental waveforms in a short time interval. The quality of the PSA algorithm can be tested by comparing the basis signals with experimental data taken in well-defined positions or, in a less direct but practically faster way, by running in-beam experiments with fast moving nuclei and by checking the Doppler correction capabilities.

An algorithm commonly used is the adaptive grid search (AGS) [25]. Basically this algorithm compares the measured signals (net and transient signals of the segments) and calculated ones over a fine grid of points in the crystal. It is suited for searching one or two interaction points per segment. It has been demonstrated that searching one interaction point in a segment is equivalent to consider the energetic barycenter if multiple hits occur, which implies that the signals vary approximately linearly in small distances. The signal comparison is done evaluating the residue R defined as the sum of the squared difference between measured and calculated signals. The algorithm evaluates R over all the points belonging to the real segment, i.e., working as a full grid search. The smallest R identifies the three-dimensional coordinates of the interaction point searched. When two points are searched, the signal in the comparison is a linear combination of signals for two possible points in the real segment, while their amplitudes represent the energy division between the two depositions. This part of data analysis is the bottleneck of the data processing, taking typically up to 95% of the computing resources. To improve the processing time, the PSA algorithm used in AGATA implement the AGS. This is a simple two-step analysis which starts with an evaluation of the residue R on a coarse grid of points and then proceeds with a search on the fine grid in the surroundings of the coarse-grid minimum to refine the position of the interaction point. With a spacing of 2 mm, the full fine grid search implies the evaluation of ≈ 1000 points in a

typical AGATA detector segment, resulting in an analysis rate of ≈ 100 events/s in a standard modern CPU. With a coarse grid spacing of 6 mm, the AGS improves the analysis speed by about one order of magnitude, without significant loss of precision. Due to its relative simplicity and its speed of execution, this algorithm is adopted in the standard PSA procedures of the AGATA collaboration and has been used in [26] to obtain a position resolution of 4 mm for γ rays of 1.4 MeV.

5.2.2.1 Radiation Damage by Fast Neutrons

One of the “by-products” of the PSA consists on the correction of the effects produced by the damage of the crystal structure caused by the interaction of fast neutrons in the germanium medium [17]. It is well-known that germanium detectors are sensitive to radiation damage induced by fast neutrons (with energy $E > 1$ keV), which generate charged lattice defects that act as trapping sites for the charge carriers [27]. This problem leads to a worsening of the energy resolution, especially in the form of a tail on the left side of the γ peak in the energy spectrum, as a result of a reduction of the charge collection efficiency (see Fig. 1 in [27] as an example). The main reason for choosing n-type crystals for the detectors used for in-beam γ -ray spectroscopy is that they appear to be less sensitive to neutron damage than p-type ones. This is due to the fact that the defects produced by fast neutrons in the germanium lattice are negatively charged and therefore do not trap the e-carriers which, due to the coaxial configuration of the detectors, dominate the signal formation in the positively biased central electrode, from which the signal is read out. In the case of γ -ray tracking arrays, also the signals induced in the segments of the outer electrode (cathode) are used. They are dominated by the collection of holes, and thus they are affected by charge trapping effects. Starting with undamaged detectors, for which the energy resolution is better in the segments than in the core, a few weeks of operation under beam at medium-high counting rate are sufficient to degrade the energy resolution of the segments to values that would normally require annealing of the crystals. Fortunately, the operation in position-sensitive mode of the germanium crystals offers an interesting way to contrast the trapping effects [27]. In fact, for a given level of neutron damage, the fraction of charge carriers lost in the collection process depends mainly on their travel path, the details of which can be easily obtained from the position of the interaction given by the PSA. The principle is represented in Fig. 5.8 taken from [28]. Ideally, the shape of the pulses is also affected by charge trapping, but for the usual levels of damage, this is not influencing appreciably the pulse shape analysis.

5.2.3 Digital Signal Processing

The choice of Germanium detectors for γ radiation is motivated in first place by their excellent energy resolution conjugated to high detection efficiency. Only superconducting and bolometer devices can provide better resolution than germanium, but their use for γ radiation is limited by their low efficiency and low count rate capabilities to few specific cases where large production of the decaying isotope

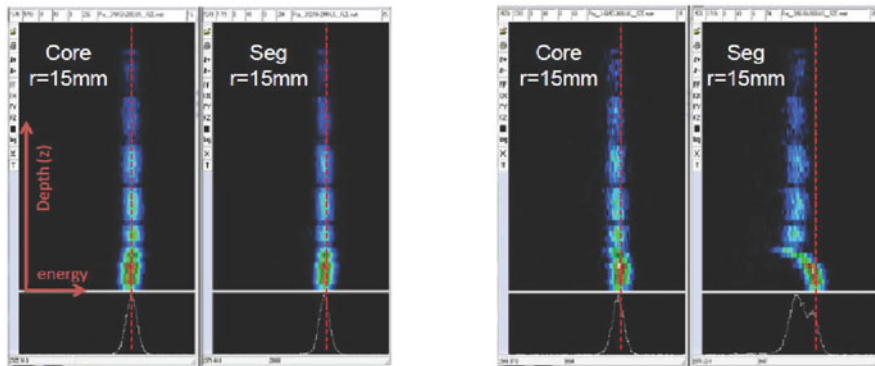


Fig. 5.8 Neutron-damage effects in a HPGe detector operated in position-sensitive mode: depth-energy correlation of the reconstructed interaction points for one of the segmented detectors used in the Legnaro AGATA Demonstrator campaign, before (left) and after (right) 3 months of beam-time operation. Taken from [28]

is available for slow, long-lasting measurements [29]. At present, germanium is the choice for spectroscopy thanks to its resolution that is the most important characteristic of the detectors. The analogue preamplified signal provided by a germanium detector requires a devoted treatment able to preserve the performance in term of intrinsic resolution.

Starting from the late 1980s, the progress in the FADC (*flash analog to digital converter*) technology made possible signal digitization with the needed dynamic range, frequency, and linearity. While a signal bandwidth sufficient to preserve the positional information from pulse shape was estimated to be of the order of 25 MHz [30], in order to obtain an optimal time resolution, a 100 MHz sampling frequency is needed. 100 MHz-FADC with 12 effective bits and sufficient linearity are commercially available nowadays.

Optimal noise filtering is essential to obtain the desired energy resolution. In general, noise filtering requires a change of shape of the detector signal. To ensure full charge collection (in the 100 ns to 500 ns time range), real implementations of preamplifiers transform the current pulse due to charge collection in a voltage signal with a considerably longer exponential shape, with a decay constant of 50 μ s. This long decay constant implies that for rates of γ detection in the order of tens of kHz, the waveform for which we need to measure the amplitude in general will seat on the tail of a previous pulse as reported in Fig. 5.9. Each pulse will be superimposed on the residual tail of the former one. The signals need to be elaborated to remove the dependence of the amplitude on the tail, and a possible solution that is commonly used in digital shaping is a waveform formation on a trapezoidal shape. With this processing, the pulses obtain a shape with a much shorter total length but in a way that preserve the proportionality of the amplitude of the signal to the energy deposited in the detector.

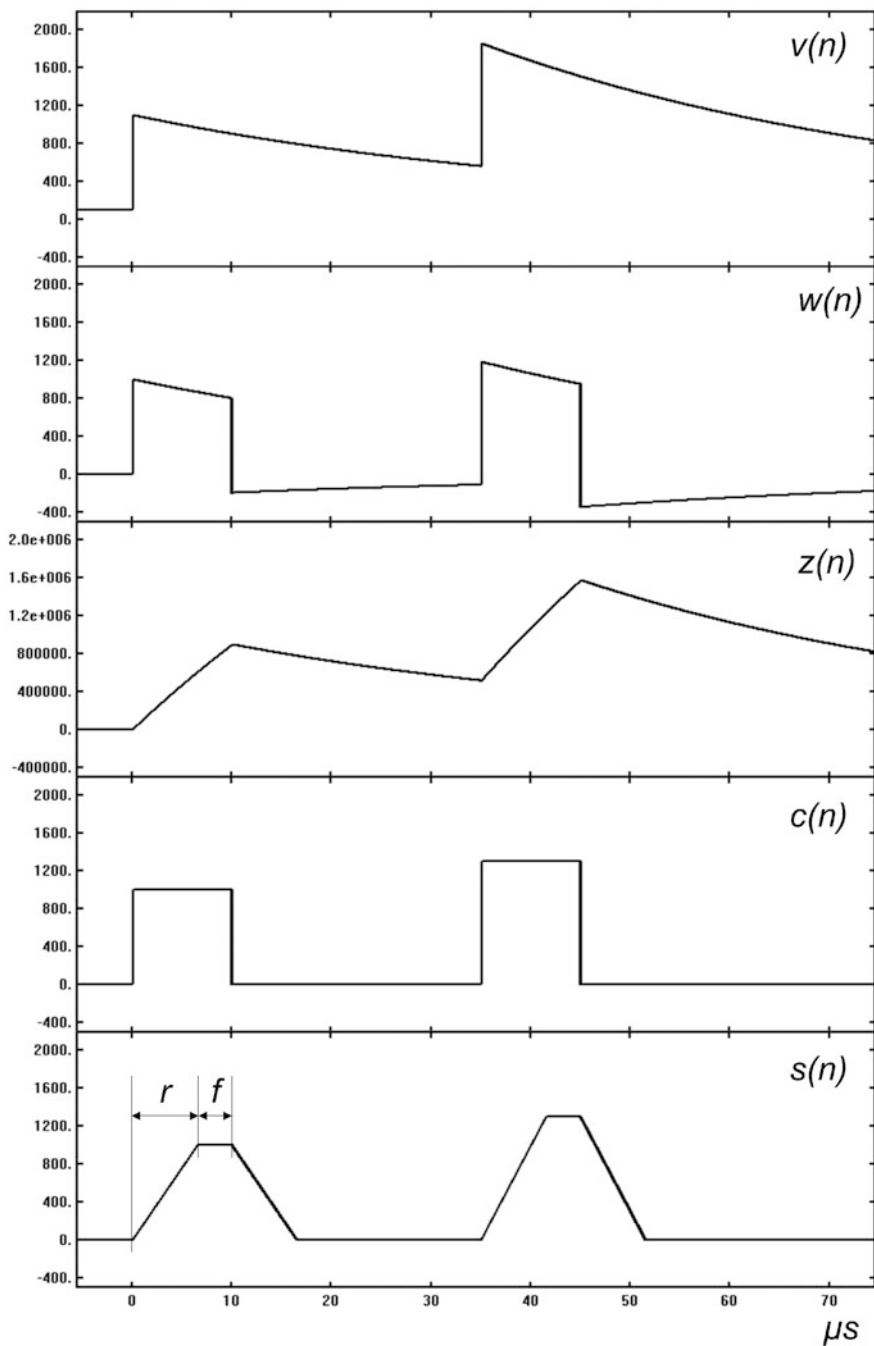


Fig. 5.9 The steps involved in the synthesis of the trapezoidal filter in the time domain as reported in (5.4). Risetime (r) and flattop (f) are defined as depicted in the bottom part of the figure

The first reported implementation of a trapezoidal filter dates back to 1968 by V. Radeka [31]. The problem of optimum signal processing for pulse amplitude spectrometry highlighted the importance of a well-defined weighting function for given noise and rate conditions. The signal and noise can be defined in a conventional way considering a detector signal, for purposes of noise analysis, as an impulse of current. The finite width of the signal is taken later into account. In a simplified scheme, two basic equivalent generators of white noise can be considered in the system. One is a current generator in parallel with the input, representing thermal noise of resistors and dielectrics and the leakage current shot noise. White noise can be represented as a random sequence of impulses, and therefore this noise is for signal processing of the same nature as the signal. The other is the equivalent noise voltage generator in series with the input, representing the overall amplifier noise. This series voltage generator can be converted into a parallel current generator producing equal noise voltage on the input capacitance. The noise-corner time constant is a measure of relative importance of the two noise generators.

Large efficiency germanium arrays are obtained by using large germanium detectors in order to minimize passive material. For example, the crystals of detectors composing the AGATA array have a volume of 370 cm³. That implies long collection time as well as large detector capacities. In order to obtain a good resolution, it is important to have a constant weighting during charge collection. This implies the use of filters with a weighting function very long with respect to the collection time, i.e., by a long filter time constant [32].

The optimum weighting function for the noise encountered in present detector-FET amplifier systems, and under the constraint of finite measurement time per event, is a cusp [32].

As reported by Jordanov and collaborators [33] with the advent of fast, high-resolution, and high linearity digitizers in the 1990s, the realization of digital filters became practical. To this purpose the trapezoidal filter was implemented to convert a digitized exponential pulse $v(n)$ into a symmetrical trapezoidal pulse $s(n)$:

$$\begin{aligned}
 w(n) &= v(n) - v(n - r - f) \\
 z(n) &= z(n - 1) + w(n) \\
 c(n) &= w(n) + M \cdot z(n - 1) \\
 s(n) &= s(n - 1) + c(n) - c(n - r)
 \end{aligned}
 \tag{5.4}$$

where r is the length of the risetime and f is the length of the flattop of the trapezoid in digitizer clock cycle units; see Fig. 5.9. The parameter M depends only on the decay time constant τ of the exponential pulse, and it is given in clock cycle units:

$$M = 1 - \exp\left(-\frac{1}{\tau}\right).
 \tag{5.5}$$

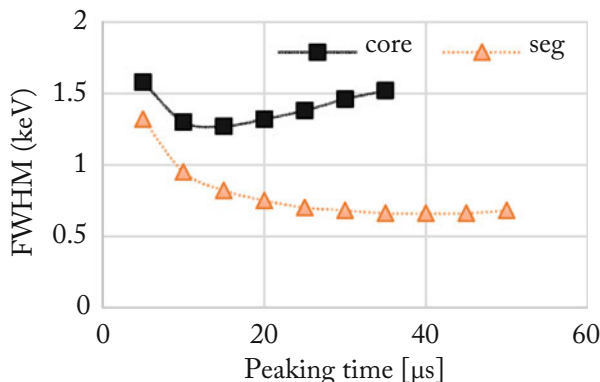


Fig. 5.10 Resolutions obtained for different peaking time of the shaper applied to the central contact (core) and to a segment (seg) of an AGATA detector, in the low energy limit

This effect of this kind of shaping is represented in Fig. 5.9 where examples of input and output signals are depicted. It is remarkable for the implementation in real-time processing electronics that the operations reported in (5.4) are all simple sums or subtractions, with the only exception of the multiplication by the constant M , (5.5). These kind of operations are cheap in terms of computing resources and can be implemented in FPGA.

The trapezoidal filter that optimizes the resolution has to be tuned as a function of the noise spectrum. The larger the capacitance of the detection element, the larger will be the integration of the low-frequency noise. As a consequence, in segmented germanium detectors, the compromise to be adopted to obtain the best possible resolution, in the low-count rate conditions, will be different for the filter used on the signals of the segments (low capacity) with respect to the one used for the central contact. In Fig. 5.10 the resolution of a segment and the resolution of the central contact of an AGATA detector are compared as a function of the peaking time (risetime + flat-top of the trapezoid).

The response function to a trapezoidal filter and the weight that is given to signal and noise can be analyzed in the frequency domain. While filtering in time domain implies performing a convolution of experimental noise with impulse response of the shaper, filtering in the frequency domain can be represented by the multiplication of the Fourier transform of experimental noise with the Fourier transform of the impulse response of the shaper.

In Fig. 5.11 a noise spectrum is reported as measured from an AGATA detector. The effect of trapezoidal filtering is visible in the same figure. The filtered spectrum was obtained multiplying the noise spectrum by the Fourier transform of the impulse response function of the trapezoidal filter.

Further filtering of the noise is obtainable using a time variant baseline restorer that consists in a long timescale running average over the input signal. This is needed to get rid of excess low-frequency noise, and it is demonstrated to be beneficial in

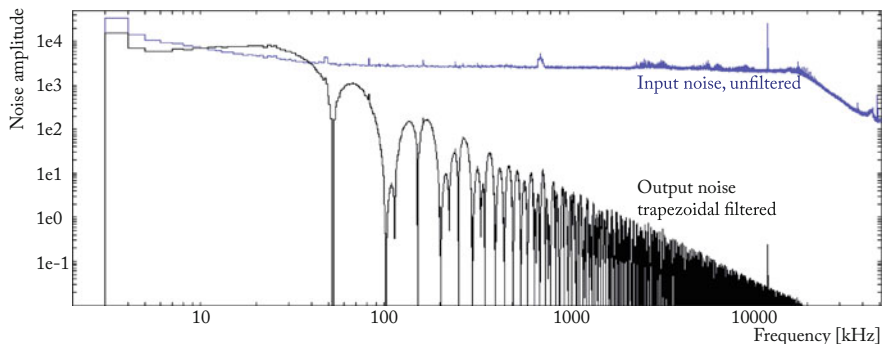


Fig. 5.11 Example of trapezoidal filtering on the noise of an AGATA detector, represented in the frequency domain. The fast Fourier transform of the input noise is depicted in blue. The output noise after the trapezoidal filtering is depicted in black

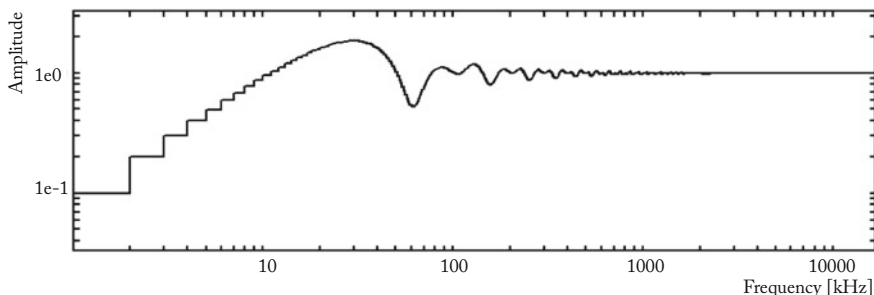


Fig. 5.12 Effect of baseline restorer filter in the frequency domain. For a running average baseline restorer of $10 \mu\text{s}$ length, the frequencies below 10 kHz result suppressed

actual systems. In the low count rate limit, the effect of the noise suppression by the baseline restorer filter is represented in Fig. 5.12 in the frequency domain.

It should be remarked that real implementations of the amplification network commonly result in a non-ideal shaping of the signal. Stray inductive and capacity couplings often result in distortions of the preamplifier response function (e.g., overshoots) that differs from a simple exponential function. Non-exponential response function impacts the outcome of the trapezoidal filtering and calls for compensating filters like anti-overshoot in the output of the preamplifier or more complex filtering based on multi-pole deconvolution.

5.2.4 Count Rate Capabilities

The performance of a γ -ray spectrometer based on digital electronics has a strong dependence on the count rate. Each individual detector of a tracking array covers a

larger solid angle than previous generation of Compton-suppressed array. Moreover, until the 4π array will not be completed, it is convenient to use the array in a closer configuration with respect to the nominal position (at 23 cm distance from the target in the case of AGATA). This allows to achieve high efficiencies at the cost of a larger count rate in each detection element, concentrating all the germanium detectors in the small fraction of solid angle around the target. In order to get the very best energy resolutions, large-volume germanium detectors are operated at low counting rates and relatively large shaping times. Therefore, we have to carefully consider the efficiency and energy-resolution losses that can arise at counting rates of 50 kHz or higher.

In order to study this effect, a measurement of the efficiency has been performed using a simplified version of the “two-sources-method” [17]. Six different measurement configurations of the two sources, ^{60}Co and ^{137}Cs , have been used. The ^{60}Co source was kept in the same position for all the runs in order to measure the resolution and the efficiency, while the ^{137}Cs source was moved to vary the total counting rate of the crystal between 13 kHz (corresponding to the ^{60}Co source alone) and 200 kHz. For every position of the sources (i.e., count rate), a scan of the possible values of the shaping time and baseline restorer width was performed. Resolution was measured for different values of the trapezoidal-filter risetime in the range between 1.25 and 10 μs and of the baseline-restorer width in the range between 0.64 and 20.48 μs . The flat top of the trapezoid was kept at 1 μs for all measurements.

Resolution strongly depends on the count rate as can be seen in Fig. 5.13 where the resolution is reported as a function of the shaping time and the baseline restorer length. Using this graphs, it is possible to optimize the response of the detectors for the actual count rate of each experiment.

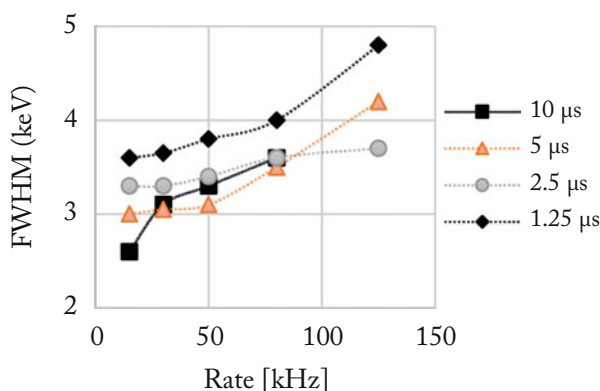


Fig. 5.13 Resolution at energy 1332.5 keV versus count rate for several trapezoidal-filter risetimes from 1.25 to 10 μs . The baseline restorer lengths was optimized for each case, resulting in 20 μs for all rates but the largest one, where the best resolution is found for a baseline restorer of 10 μs

5.3 Doppler Correction Capabilities

It is of foremost interest to have the best possible Doppler corrections capabilities. For this reason in-beam experiment performance of a γ -ray tracking array like AGATA depends critically on the precision achieved in locating the individual photon interaction points.

An experiment using the first prototype of AGATA triple cluster was performed, in order to compare the performance of different pulse shape analysis algorithms under realistic experimental conditions.

The basic idea is that, when the γ rays are emitted in-flight by a recoiling nucleus, the width of peaks in the Doppler-corrected spectra will depend on three factors, namely, the intrinsic detector energy resolution, the error on the velocity vector of the emitting nucleus, and the uncertainty on the photon direction. The last factor depends on the position resolution of the PSA algorithm used. If the other causes of Doppler broadening are known, the position resolution of the detector can be inferred from the observed energy resolution. This is not an easy task because all the direct and indirect sources of Doppler broadening have to be tracked down and, when not negligible, accurately quantified.

The broadening of the peaks has been predicted using a Monte Carlo simulation, but, as a first approximation, it can also be calculated using the propagation of errors and some schematic assumptions. The importance of this approach is to make the results intuitive. The Doppler-shift formula is the following:

$$E_{\gamma}^{cm} = E_{\gamma} \frac{1 - \beta \cos \theta}{\sqrt{1 - \beta^2}} \quad (5.6)$$

where E_{γ}^{cm} is the intrinsic energy of the γ -ray, E_{γ} is the energy of the photon in the laboratory (in other words the energy seen by the detector), β is the velocity of the emitting nucleus, and θ is the angle between the direction of the recoiling nucleus and the direction of the photon in the laboratory.

Each of the parameters entering the formula contributes to the final uncertainty. For instance, the θ angle is determined experimentally from the position of the first interaction of the photon and the target position. Thus, an error in the position is translated into an error in the direction of the γ -ray, giving an imperfect Doppler correction. Quantitatively, the contribution of each parameter to the final position resolution is evaluated through the propagation of errors on E_{γ}^{cm} , giving:

$$\begin{aligned} (\Delta E_{\gamma}^{cm})^2 &= \left(\frac{\partial E_{\gamma}^{cm}}{\partial \theta} \right)^2 (\Delta \theta)^2 + \\ &+ \left(\frac{\partial E_{\gamma}^{cm}}{\partial \beta} \right)^2 (\Delta \beta)^2 + \\ &+ \left(\frac{\partial E_{\gamma}^{cm}}{\partial E_{\gamma}} \right)^2 (\Delta E_{\gamma})^2. \end{aligned} \quad (5.7)$$

In this calculation, the different broadening sources are considered as statistically independent contributions, neglecting for simplicity any correlation between them. In (5.7), $\Delta\beta$ and $\Delta\theta$ are, respectively, the uncertainty on the velocity module and on the direction of the nucleus emitting the radiation. Even if the recoil velocity vector can be measured on an event-by-event basis, $\Delta\beta$ and $\Delta\theta$ will be generally non-zero.

The term ΔE_γ in (5.7) describes the contribution of the intrinsic energy resolution of the detector.

The partial derivatives are:

$$\begin{aligned}\frac{\partial E_\gamma^{cm}}{\partial\theta} &= E_\gamma \frac{\beta \sin\theta}{\sqrt{1-\beta^2}} \\ \frac{\partial E_\gamma^{cm}}{\partial\beta} &= E_\gamma \frac{\beta - \cos\theta}{(1-\beta^2)^{3/2}} \\ \frac{\partial E_\gamma^{cm}}{\partial E_\gamma} &= \frac{1 - \beta \cos\theta}{\sqrt{1-\beta^2}}\end{aligned}\tag{5.8}$$

The angular error is propagated to the error in the determination of the intrinsic energy of the γ ray by the coefficient given in the first row of (5.8). As an example, the contributions of the three sources of Doppler broadening are sketched in Fig. 5.14, for the case of photons of 1 MeV emitted from a nucleus in motion with $\beta = 0.2\%$ and detected with an uncertainty $\Delta\theta = 1^\circ$ on its direction.

Besides the finite resolution on the position of the interaction, in an indirect measurement, the other relevant sources of error in the determination of the intrinsic energy of the photon are the energy resolution of the detector and the uncertainty on the velocity vector of the emitting recoil. To simplify the experimental setup, it is possible to measure indirectly the velocity vector of the emitting nucleus through a kinematic calculation based on the measurement of the velocity vector of the other reaction products. As a consequence, some other contributions have to be considered to explain the experimental broadening, namely:

- angular and energy dispersion of beam due to the accelerator and the transport;
- straggling of the beam and reaction products inside the target.

The position resolution provided by the PSA algorithm can be deduced from the quality of the Doppler correction, provided a proper reaction is selected to maximize the Doppler broadening originating from the position resolution and to minimize the other sources. A reaction that was used to investigate this was the $^{48}\text{Ti}(d, p)$ in inverse kinematics [26].

The results of this procedure are shown in Fig. 5.15, together with the spectra obtained by Doppler correcting at detector or segment level. The improvement in quality of the spectra is apparent. For the 1382 keV peak of ^{49}Ti , FWHM=4.8 keV is obtained following the PSA algorithm, which should be compared to 14 keV and 35 keV at segment and detector level, respectively.

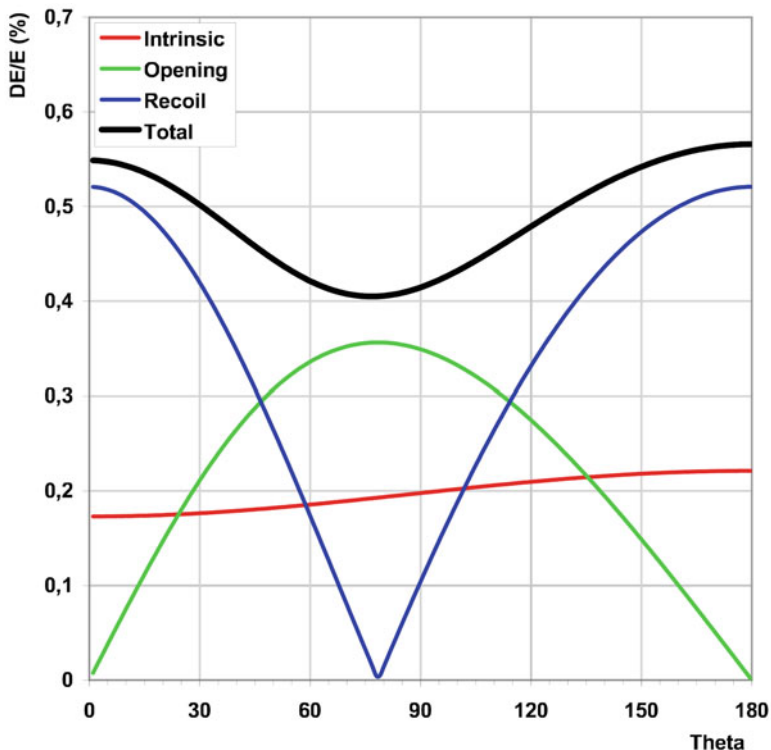


Fig. 5.14 The contributions of the different Doppler broadening sources as a function of the azimuthal angle of the detector with respect to the direction of the recoil emitting the radiation. A photon energy of 1 MeV is assumed, with a typical energy resolution for a germanium detector, producing the “Intrinsic” contribution (in red); a source velocity of $\beta = 20.0\%$ with an error of 0.5%, giving the “Recoil” contribution (in blue); an uncertainty $\Delta\theta = 1^\circ$ in the source direction, obtaining the “Opening” contribution (in green)

The resulting position resolution is extracted quantitatively by comparing the experimental peak width to the simulated value using the curves shown in Fig. 5.15. In this case the simulated data from the three individual crystals were summed up, obtaining the curve plotted in Fig. 5.16. The observed FWHM of 4.8 keV of the peak at 1382 keV corresponds to a position resolution of 3.8 mm at this energy.

The improvement in Doppler correction capabilities have been exploited, for example, in beam-induced fission experiments at GANIL, using the VAMOS magnetic spectrometer for fission fragment identification and velocity reconstruction. In Fig. 5.17 the comparison of the Doppler corrected spectrum for ^{98}Zr obtained with a standard HPGe array (EXOAM) and AGATA is shown. Already from such preliminary analysis of the commissioning data, a gain in energy resolution is evident.

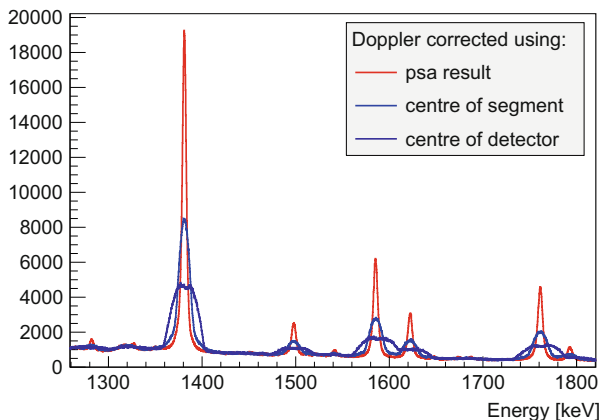


Fig. 5.15 Doppler-corrected spectra for the full cluster, deducing the direction of the photon, respectively, from the center of the detector, center of the segment, and the PSA information. Taken from [34]

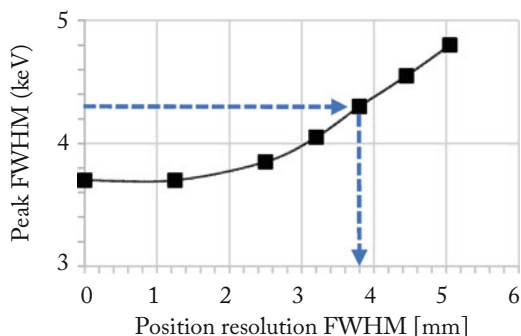


Fig. 5.16 Width of the simulated 1382 keV peak as a function of the position smearing for the full triple cluster. Individual crystal energy resolution have been considered. The horizontal arrow indicates the experimental width. Taken from [34]

5.4 Lifetime Measurements with Doppler Techniques

The lifetime of a nuclear state is the observable that is measured in γ -ray spectroscopy experiments in order to derive the reduced transition probabilities, crucial for the comparison with nuclear theoretical models. The Doppler-shift techniques are powerful tools for lifetimes in the 10^{-14} – 10^{10} s interval. When the nuclear level of interest is populated in a heavy-ion reaction, the radioactive decay will happen from the moving reaction product. The finite time it takes to travel a given distance can be considered as a “unit of measurement” of the decay lifetime of the populated level. When the radiation with energy E_γ (center of mass energy) is emitted by a nucleus moving with a velocity $\beta = v/c$, the γ -ray energy observed

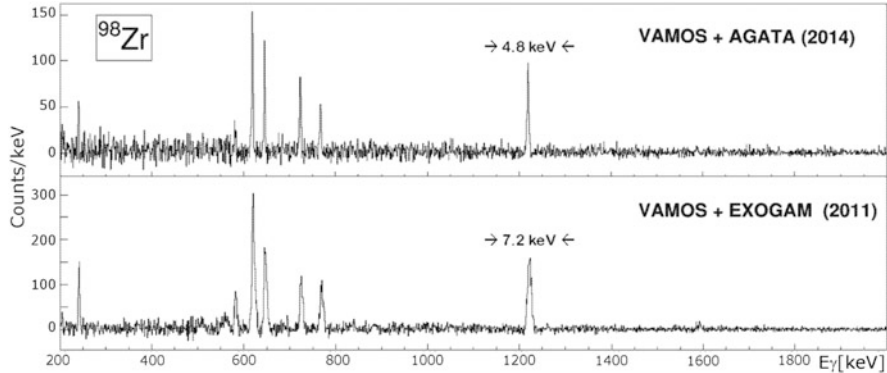


Fig. 5.17 Doppler correction capabilities in the AGATA+VAMOS campaign at GANIL. The Doppler-corrected spectra corresponding to ^{98}Zr (selected in VAMOS) obtained with AGATA (upper panel) and EXOGAM (lower panel) reveal the improvement due to the AGATA position resolution

at an angle θ between the recoil and the γ -ray emission directions follows the Doppler relation. Depending on the order of magnitude of the lifetime and on the kind of nuclear reaction involved, different variants of the technique have been developed. All methods take great advantage of the use of HPGe detectors, whose excellent energy resolution allows for the observation of fine details in the γ energy spectrum. In particular, a big improvement in the accuracy of the determination of the lifetimes by means of these techniques was achieved with the use of arrays of HPGe detectors, placed symmetrically all around the target position. The possibility of a simultaneous measurement at many angles is important for discovering the presence of contaminants as well as for increasing the accuracy since the lifetime is obtained in a number of independent evaluations. When the lifetime of the level of interest is comparable to the slowing down time of the emitting nucleus in a given material, the Doppler-shift attenuation method (DSAM) is used. This technique is widely adopted for the measurement of sub-ps lifetimes, corresponding to the typical slowing down times of heavy ions in solid mediums, which are $\approx 10^{-13}$ – 10^{-12} s for kinetic energies below or about 10 MeV per nucleon. Thanks to the angular resolution of a tracking array as AGATA, this technique can be pushed to shorter lifetimes. In case of lifetimes of few fs, the shape of the peak in the γ spectrum is mainly determined by the kinematics, since most of the nuclear states decay as soon as they are populated. The first experiment performed with the AGATA array to measure \approx fs lifetimes aimed to the determination of the lifetime of an excited state in ^{15}O , of interest for nuclear astrophysics. The details of the experiment are reported in [35]. In Fig. 5.18 the effect on the observed peak position of different lifetimes is shown in the “AGATA-like” case and in a standard coaxial detector. As evident from the picture, the extremely good angular resolution allows for distinguishing among the different lifetimes. Such angular sensitivity for γ rays de-exciting short-lived levels is depicted in Fig. 5.19, where the observation angle is

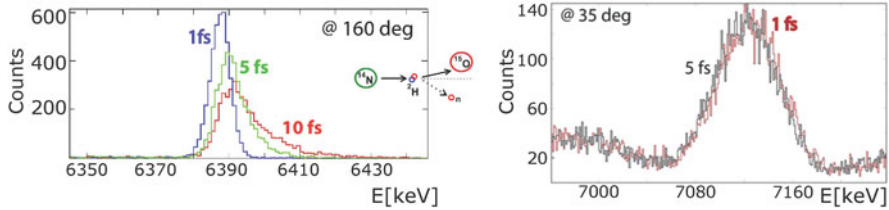


Fig. 5.18 Examples of sensitivity to fs lifetimes. 6.79 MeV γ -rays emitted by ^{15}O nuclei produced in the simplify direct process reported in the figure, with the produced ^{15}O recoiling at a fixed direction with respect to the beam axis (35 deg). The sensitivity to \approx fs lifetimes obtained in the spectra of AGATA (left) is lost when using a traditional HPGe detector, as one from the GASP array (right). Taken from [35]

sorted as a function of the detected energy. The broadening of the γ -ray peaks due to short lifetimes is evident as compared to the γ rays emitted at rest. Such line shapes can be analyzed by means of Geant4 simulations in order to extract the lifetime. In order to establish the very lower limit of sensitivity of the measurement, Geant4 simulations of the whole production, slowing down, gamma emission, and detection process can be used. For the specific experiment considered here as an example, one obtains the χ^2 curves reported in Fig. 5.20. Those curves are useful to establish the minimum value of lifetime that one can reach with a given setup. In the considered case, one sees the appearance of a minimum in the χ^2 curve for lifetimes of about 0.7 fs.

5.5 Linear Polarization Measurements

The “almost continuous” angular distribution achievable with tracking arrays can be exploited to gain a new degree of sensitivity in γ polarization measurements, necessary for the determination of the magnetic or electric character of γ transitions and, thus, of the parity of nuclear states. Clover detectors (see Sect. 5.1) are usually used for such measurements [36], by evaluating the asymmetry A_S of the Compton scattering of γ rays corresponding to a given transition inside the clover detector. This asymmetry is typically evaluated with respect to the reaction plane, and it is given by:

$$A_S = \frac{N_{\parallel} - N_{\perp}}{N_{\parallel} + N_{\perp}} \quad (5.9)$$

where N_{\parallel} and N_{\perp} are the number of Compton scattered γ rays detected, respectively, parallel and perpendicular to the reaction plane.

Using the tracking capabilities of arrays as AGATA, the azimuthal Compton scattering angle ϕ can be evaluated with a 1 degree precision, as shown in Fig. 5.18. The linear polarization can be thus determined, instead of using (5.9), by considering that the average Compton scattering cross section depends on ϕ via

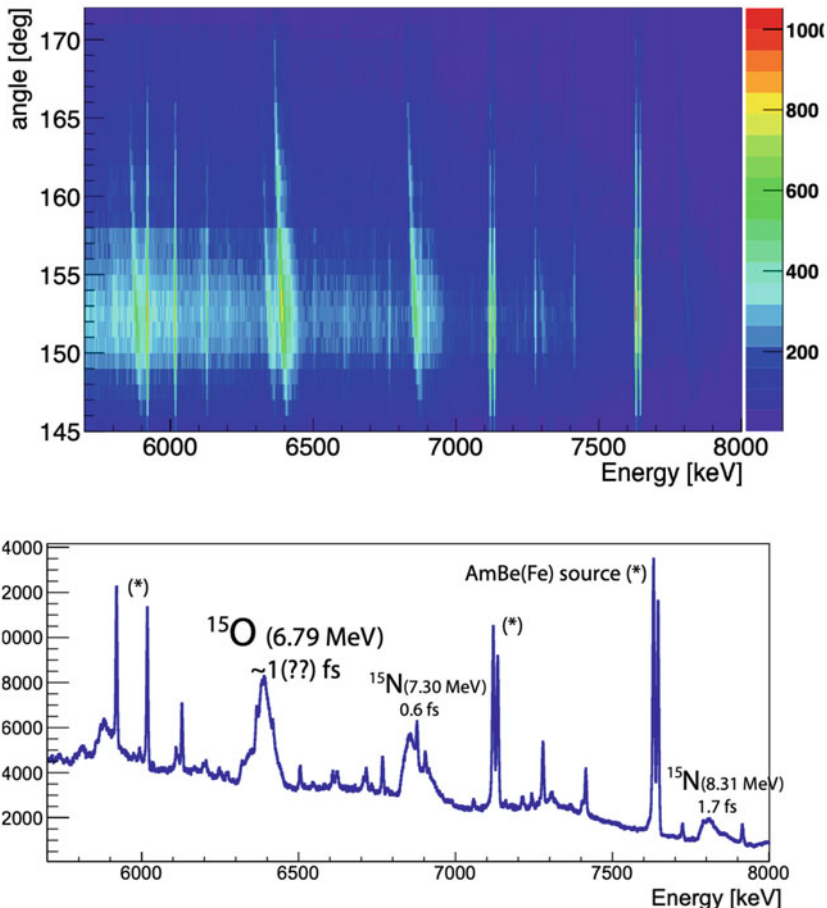


Fig. 5.19 Angular position of the first interaction point, with respect to the beam direction, sorted as a function of the energy of the reconstructed γ ray. The narrow straight lines correspond to the emission at rest from the AmBe(Fe) source, while the broad “tilted” lines are gammas emitted while the excited nucleus is moving in the stopper. In the projection on the energy axis (lower panel), the broad and composite structure are assigned to ^{15}O and ^{15}N , produced in the reaction. Taken from [35]

the relation [37]:

$$N(\phi) = a + b \cos(2\phi) \tag{5.10}$$

The analyzing power on the AGATA triple clusters for γ linear polarization has been determined in [37] using (5.10). The measured $N(\phi)$, normalized to an isotropic distribution obtained with ^{137}Cs calibration source, is reported in Fig. 5.21 for the $2^+ \rightarrow 0^+$ transitions in $^{106,108}\text{Pd}$ populated in Coulomb excitation experiments. The impact of position resolution and other systematic effects is discussed in [37].

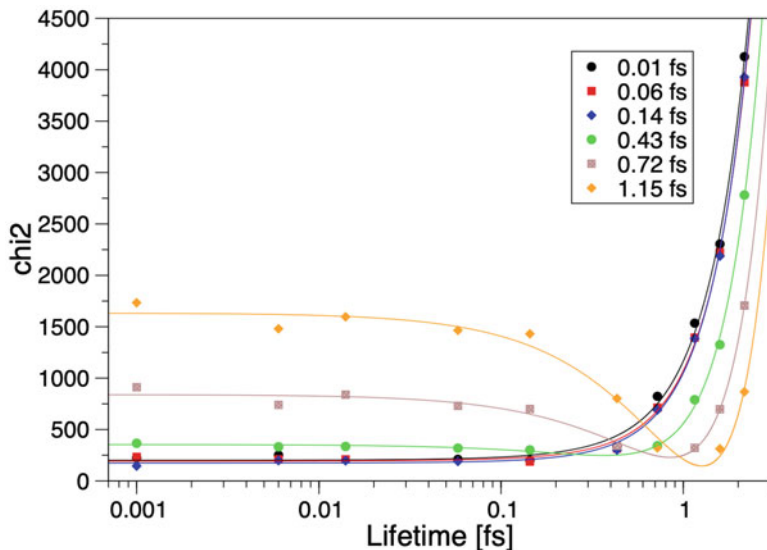


Fig. 5.20 Sensitivity of the simulated line shape to changes of the lifetime in the fs region, for the experiment considered in the text. A minimum in the χ^2 curve starts being evident for lifetimes around 0.7fs. Taken from [35]

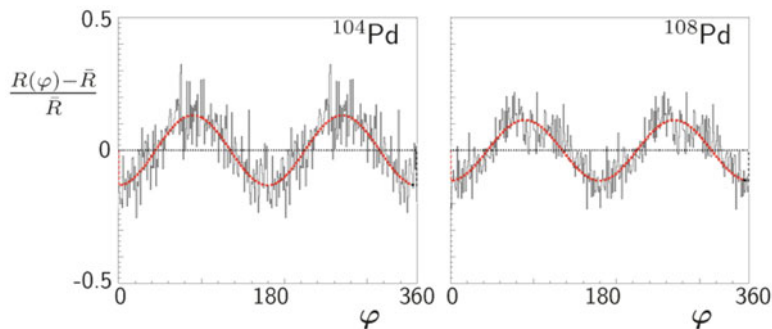


Fig. 5.21 Asymmetry distribution for the $2^+ \rightarrow 0^+$ transitions in $^{106,108}\text{Pd}$ populated in Coulomb excitation experiments. The γ polarization is obtained by fitting the experimental data sorted with a binning of 1 degree, to (5.10). Taken from [37]

5.6 Conclusions

In this lecture notes, the limits of previous generation Compton-suppressed γ -detector arrays have been discussed, motivating the development and the construction of the state-of-the-art γ -tracking arrays. The basics of the techniques in use for the operation of such detectors have been presented. The tracking arrays present improved detection sensitivity, thanks to enhanced efficiency and Doppler

correction capabilities, extremely important for nuclear structure studies using low-intensity radioactive beams. Moreover, the position sensitivity of the tracking array can be exploited, not only with the aim of Doppler correction but also for gaining a new degree of sensitivity in lifetime measurements and polarization studies. In order to highlight those new capabilities, a limited selection of results has been discussed.

References

1. D. Bazzacco, Proc. Confer. Phys. Large γ -Ray Detector Arrays **32**, 376 (1992)
2. C. Rossi Alvarez, Nucl. Phys. News **3**, 10–13 (1993)
3. C.W. Beausang et al., Nucl. Instrum. Methods A **313**, 37–49 (1992)
4. J. Simpson, Zeitschrift für Physik A Hadrons Nuclei **358**(2), 358 (1997)
5. I.-Y. Lee, Nucl. Phys. A, **520**, c641–c655 (1990)
6. SPES Technical Design Report, INFN-LNL-223 (2008)
7. Th. Kroell, D. Bazzacco, Nucl. Instrum. Methods A **463**, 227–249 (2001)
8. G. Duchêne et al., Nucl. Instrum. Methods A **432**, 90–110 (1999)
9. M. Wilhelm et al., Nucl. Instrum. Methods A **381**, 462–465 (1996)
10. U. Rizwan et al., Nucl. Instrum. Methods A **820**, 126–131 (2016)
11. F. Azaiez, Nucl. Phys. A **654**, 1003c–1008c (1999)
12. C. Michelagnoli et al., EPJ Web Conf. **193**, 04009 (2018)
13. G. Colombi, Master Thesis, University of Milan and ILL (2020)
14. D. Reygadas, PhD Thesis, University of Grenoble and ILL (2021)
15. S. Akkoyun et al., Nucl. Instrum. Methods A **668**, 26–58 (2012)
16. S. Paschalis et al., Nucl. Instrum. Methods A **709**, 44–55 (2013)
17. G.F. Knoll, *Radiation Detection and Measurement*, 4th edn. (Wiley, New York, 2010)
18. G.J. Schmid et al., Nucl. Instrum. Methods A **430**, 69–83 (1999)
19. A. Lopez-Martens et al., Nucl. Instrum. Methods A **533**, 454–466 (2004)
20. L. Nelson, et al., Nucl. Instrum. Methods A **573**, 153–156 (2007)
21. T.M. Hoa, A. Korichi, *5th AGATA Week* (Orsay, 2007).
22. B. Bruyneel et al., Eur. Phys. J. A **52**, 70 (2016)
23. B. Bruyneel, PhD Thesis, University of Cologne (2006)
24. B. Bruyneel, P. Reiter, G. Pascovici, Nucl. Instrum. Methods A **569**, 774–789 (2006)
25. R. Venturelli, D. Bazzacco. LNL Annual Report (2005)
26. F. Recchia et al., Nucl. Instrum. Methods A **604**, 555–562 (2009)
27. B. Bruyneel et al., Eur. Phys. J. A **49**, 1–9 (2013)
28. D. Bazzacco, *4th Summer School in Radiation Detection and Measurements*, Munich (2011)
29. A. Yamaguchi et al., Phys. Rev. Lett. **123**, 222501 (2019)
30. F.C.L. Crespi et al., Nucl. Instrum. Methods A **593**, 440–447 (2008)
31. V. Radeka, IEEE Trans. Nucl. Sci. **15**, 455–470 (1968)
32. V. Radeka, Nucl. Instrum. Methods **99**, 525–539 (1972)
33. V.T. Jordanov et al., Nucl. Instrum. Methods A **353**, 261–264 (1994)
34. F. Recchia, PhD Thesis, University of Padova (2008)
35. C. Michelagnoli, PhD Thesis, University of Padova (2013)
36. L. Garcia-Rafi et al., Nucl. Instrum. Methods A **391**, 461 (1997)
37. P.G. Bizzeti et al., Eur. Phys. J. A **49**, 51 (2015)